JACS
JOURNAL OF THE AMERICAN CHEMICAL SOCIETY

Communication

pubs.acs.org/JACS

$[Au_7]^{3+}$: A Missing Link in the Four-Electron Gold Cluster Family

Yukatsu Shichibu,[†,‡] Mingzhe Zhang,[†] Yutaro Kamei,[†] and Katsuaki Konishi*[,†,‡]

[†]Graduate School of Environmental Science and [‡]Faculty of Environmental Earth Science, Hokkaido University, North 10 West 5, Sapporo 060-0810 Japan

Supporting Information

ABSTRACT: Ligand-stabilized ultrasmall gold clusters offer a library of diverse geometrical and electronic structures. Among them, clusters with four valence electrons form an exceptional but interesting family because of their unique geometrical structures and optical properties. Here, we report a novel diphosphine-ligated four-electron Au_7 cluster (**2**). In good agreement with previous theoretical predictions, **2** has a "core+*one*" structure to exhibit a prolate shape. The absorption spectrum showed an isolated band, similar to the spectra of Au_6 and Au_8 clusters with "core+*two*" structures. TD-DFT studies demonstrated that the attachment of only one gold atom to a polyhedral core is sufficient to generate unique electronic structures and characteristic absorptions. The present result fills the missing link between Au_6 and Au_8 in the four-electron cluster family, showing that the HOMO−LUMO gap increases with increasing nuclearity in the case of the tetrahedron-based "core+*exo*" clusters.

Ligand-protected gold nanoclusters with defined nuclearity and geometrical structures have been a topic of considerable interest because of their structure-dependent optical/electronic properties.[1] The electron counting rule, which was originally introduced by Mingos[2,3] and has been developed as the superatom concept,[4] is useful for elucidating the inherent stability, geometrical structures, and chemical nature of cluster compounds. For cluster compounds formulated as $[Au_NL_SX_M]^z$ (L: neutral ligand, X: anionic ligand), the count of 6s electrons in the metallic moiety ($n^* = N - M - z$) is correlated with the closed-shell requirements, and its validity has been actually demonstrated for various phosphine-[3,5] and thiolate-ligated clusters.[6] For the phosphine-coordinated family, numerous examples of structurally characterized cationic clusters have been reported in the literature.[7] Most clusters have $n^* = 6$ (e.g., $[Au_9]^{3+}$)[8] or $n^* = 8$ (e.g., $[Au_{13}]^{5+}$)[9] electron systems, which match the criteria of the electron counting concept. However, some lower-nuclearity clusters are known to have exceptional four-electron systems ($n^* = 4$). These clusters have unusual tetrahedron-based geometries and are characterized by unique optical properties; however, the examples have been limited for $[Au_6]^{2+}$ [10,11] and $[Au_8]^{4+}$.[12] Herein, we present the first experimental observation of intermediate $[Au_7]^{3+}$ species in the dppp-ligated cluster family ($[Au_7(dppp)_4]^{3+}$, **2**) (dppp: $Ph_2P(CH_2)_3PPh_2$) and show its tetrahedron-based prolate geometry. We also discuss the relationship between the optical properties and nuclearity for a series of four-electron clusters with "core+*exo*"-type structures.

Among phosphine-coordinated gold clusters, Au_6,[10,11] Au_8,[12−14] Au_9,[15] Au_{10},[16] and Au_{11}[17,18] are reported to take multiple geometrical forms. In contrast, only pentagonal bipyramid geometry has been observed for the Au_7 cluster, which has a monovalent six-electron system ($[Au_7]^+$).[14,19] Mingos et al. predicted the two-electron oxidation of $[Au_7]^+$ to $[Au_7]^{3+}$ ($n^* = 4$) accompanying a change in cluster geometry;[3] however, the synthesis and structural characterization of $[Au_7]^{3+}$ species have not yet been achieved. Alternatively, we observed that the four-electron $[Au_7]^{3+}$ is efficiently generated from isoelectronic $[Au_6(dppp)_4]^{2+}$ (**1**) by treatment with silver ion. Typically, when a methanol solution of $\mathbf{1}\cdot(BF_4)_2$ was treated with $AgBF_4$ or $AgNO_3$ (5 molar equiv) at room temperature, the color of the solution immediately changed from deep-blue to reddish-violet, and the absorption spectra showed a significant blue shift (584 → 556 nm). The ESI-MS spectrum of the main cluster product isolated by reprecipitation showed a set of ESI-MS signals at ∼1009, which we unambiguously assigned to the trivalent cluster cation ($[Au_7(dppp)_4]^{3+}$, **2**) through comparison with the simulated isotope pattern (Figure 1). Although **2** can be formed by simple attachment of a Au^+ ion to **1**, the absorption and ESI-MS spectra of the product of the direct reaction of **1** with $Au(PPh_3)NO_3$ or $Au(PPh_3)Cl$ gave no indication of the formation of **2**. Therefore, the interaction/reaction of **1** with Ag^+ may result in the formation of an intermediate that serves as a "naked" Au^+ donor leading to the formation of **2** by the reaction with residual **1**. Although ESI-MS signals associated with the silver-containing cluster species were not detected in the reaction mixture, the aforementioned results imply that the

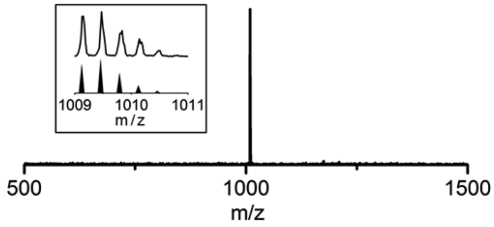

Figure 1. ESI mass spectrum of **2**. The inset shows a comparison of the experimental data with the calculated isotope pattern of $[Au_7(dppp)_4]^{3+}$.

Received: August 5, 2014
Published: September 3, 2014

   dx.doi.org/10.1021/ja508005x | J. Am. Chem. Soc. 2014, 136, 12892−12895

silver ion exhibits unique activity toward mediation of the growth/etching of gold clusters.[10]

The structure of $\mathbf{2}\cdot(BF_4)_3$ was determined by single-crystal X-ray crystallography (Figure 2a). The heptanuclear skeleton

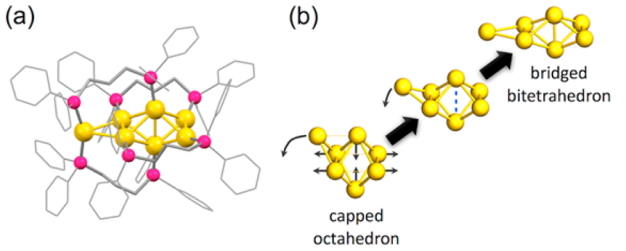

Figure 2. (a) Crystal structure of **2** and (b) schematic of the transformation of a capped octahedron into a bridged bitetrahedron ("core+*one*" geometry).

had an edge-bridged bitetrahedral geometry, which can be depicted as a "single-*exo*" version of a $[Au_8]^{4+}$ cluster with a bitetrahedral Au_6 core and two *exo* gold atoms ($[Au_8(dppp)_4X_2]^{2+}$ (**3**, X = Cl or alkynyl))[12] (Figure 3). In

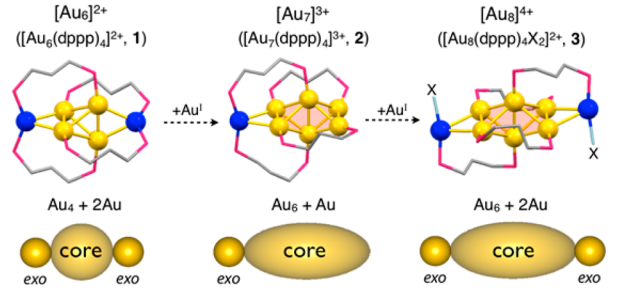

Figure 3. Schematic of the geometrical structures of the gold moieties of **1**–**3**; **2** and **3** are formally formed by a growth reaction from **1** by successive addition of gold(I) ions.

addition, the structure can be described as a derivative of **1**, where one of the two terminal triangles of **1** forms a tetrahedron by accommodating an additional gold atom. The Au–Au bond distances involving the *exo* gold atoms of **2** are 2.899 and 2.948 Å, which fall between those of **1** (2.798 Å) and **3** (X = Cl) (2.970–3.072 Å). As commonly observed in the "core+*two*"-type clusters (**1**,[11] **3**,[12] and $[Au_{11}(dppe)_6]^{3+}$),[18] the *exo* gold atom of **2** is bonded to two ligands, whereas the other six gold atoms comprising the bitetrahedron accommodate a single phosphine ligand. Consequently, the cluster units of **1**–**3**, though having different nuclearity, are coordinated by the same number (8) of phosphorus atoms (Figure 3).

As shown in Figures 2a and 3, the gold framework of the $[Au_7]^{3+}$ cluster (**2**) exhibits a prolate shape similar to those of known four-electron clusters ($n^* = 4$) such as $[Au_6(PPh_3)_6]^{2+}$ (bitetrahedron),[10] **1** (tetrahedron + *exo* × 2),[11] and **3** (bitetrahedron + *exo* × 2).[12] Mingos rationalized the cluster geometry on the basis of the structural jellium model and claimed that four valence electrons have ground-state configurations of $[1S^{\sigma}]^2[1P^{\sigma}]^2$ to favor prolate geometry.[3] In this respect, the structure of **2** agrees with the model, supporting the hypothesis that a prolate shape is a common feature of $n^* = 4$ clusters. Mingos also suggested a capped octahedron as the prolate geometry of the $[Au_7]^{3+}$ cluster,[3] which is apparently different from the bridged bitetrahedral geometry we observed for the Au_7 skeleton of **2**. However, a capped octahedron can be transformed into a bridged bitetrahedron via some modifications (Figure 2b), indicating that the chelating effect of the diphosphine ligand plays a critical factor role in determining the cluster geometry.

In previous papers, we reported that the absorption spectra of "core+*two*"-type gold clusters bearing *two exo*-attached gold atoms (**1**, **3**, and $[Au_{11}(dppe)_6]^{3+}$) commonly exhibit single isolated absorption bands in the visible region.[20] This feature is characteristic of these clusters because such optical profiles are not observed for conventional polyhedral clusters. TD-DFT studies of the "core+*two*" clusters have indicated that their HOMO and LUMO are localized around the bridged polyhedral edge and *exo* gold atoms and that the HOMO–LUMO transitions critically contribute to the appearance of the isolated visible bands. However, it is not certain whether *two exo* atoms are required to generate these unique optical properties. DFT calculations of the "core+*one*"-type $[Au_7]^{3+}$ cluster were examined for the nonphenyl derivative of **2** ($[Au_7(H_2P(CH_2)_3PH_2)_4]^{3+}$, **2′**), which revealed that the overall orbital distribution pattern is similar to that of the "core+*two*"-type clusters. The energies of the HOMO and LUMO, both of which are mostly composed of the 6sp atomic orbitals of gold, were appreciably different from those of the closest orbitals (Figure 4a). Furthermore, TD-DFT calculations indicated that

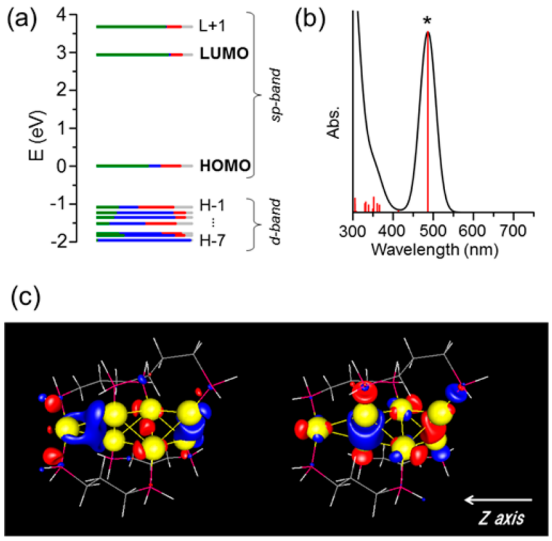

Figure 4. (a) Kohn–Sham (KS) orbital energy level diagram and (b) theoretical absorption spectrum of $[Au_7(H_2P(CH_2)_3PH_2)_4]^{3+}$ (**2′**). Each KS orbital energy is relative to the HOMO energy and is drawn to indicate the relative contributions (line lengths with color labels) of the atomic orbitals of Au (6sp) in green, Au (5d) in blue, P (3p) in red, and miscellaneous in gray. H − X and L + Y represent HOMO − X and LUMO + Y, respectively. The asterisk indicates the HOMO–LUMO transition. (c) The LUMO (left) and HOMO (right) of **2′**. The *z*-axis was chosen along the longitudinal direction of the Au_7 core.

the HOMO–LUMO transition exhibited dominant oscillator strength, resulting in an isolated absorption band at ~500 nm in the simulated spectrum (Figure 4b).[22] This spectral profile was well reproduced in the experimental spectrum. As shown in Figure 5a, $\mathbf{2}\cdot(BF_4)_3$ in methanol exhibited an isolated visible band at 556 nm. These results clearly indicate that the attachment of only one gold atom to the polyhedral core leads to the generation of unique electronic structures and optical properties.

dx.doi.org/10.1021/ja508005x | J. Am. Chem. Soc. 2014, 136, 12892–12895

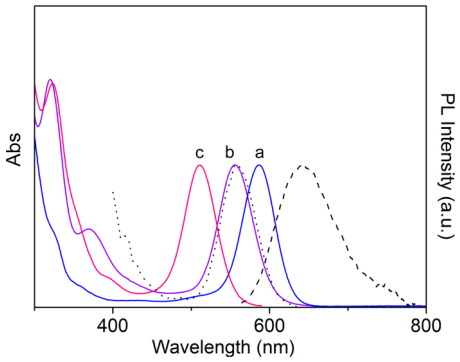

Figure 5. Absorption spectra (solid lines) of (a) **1**·$(NO_3)_2$, (b) **2**·$(BF_4)_3$, and (c) **3**·$(PF_6)_2$ (X = Cl) and photoluminescence (λ_{ex} = 555 nm) (dashed line) and excitation (λ_{em} = 642 nm) (dotted line) spectra of **2**·$(BF_4)_3$ in MeOH at 25 °C.

Frontier orbital analyses of **2′** (Figure 4c) revealed that an s-like orbital exists at the *exo*-bridged polyhedral edge in the HOMO, whereas the contribution of p_z-like orbitals directed to the *exo* atom from the polyhedron was distinctly observed in the LUMO. Thus, the valence electrons at the ground state appear dominantly localized on the polyhedral core, which was supported by DFT-based charge analyses (Table S5). Consequently, the attachment of only one gold atom leads to the generation of a HOMO and a LUMO that allow the effective core → *exo* intermetal transition. Although the HOMO and LUMO observed around the opposite terminal edge are also notable, the core → *exo* transition is likely to be preferentially responsible for the appearance of the intense visible absorption band. The molar coefficient (ε) of the visible absorption band of **2** was estimated to be 1.9×10^4 M^{-1} cm^{-1}, which is appreciably smaller than that of the "core+*two*"-type Au_8 cluster (**3**, X = Cl) (2.7×10^4 M^{-1} cm^{-1}).[20]

Figure 3 also shows a formal scheme illustrating the growth of the core+*exo*-type four-electron clusters by successive addition of a gold(I) ion to the $[Au_6]^{2+}$ cluster (**1**). As mentioned above, the electronic structures of these clusters are similar to each other; thus, a comparison of their first-excitation energies in terms of their nuclearity should be interesting. As shown in Table 1 and Figures 5 and S2, the HOMO−LUMO transition energy of $[Au_7]^{3+}$ (**2**) fell between those of $[Au_6]^{2+}$ (**1**) and $[Au_8]^{4+}$ (**3**, X = Cl) clusters, revealing a clear blue shift on the increase of the nuclearity. The lowest optical transition of colloidal metal nanoparticles generally exhibits, as a consequence of the quantum size effect, a blue shift as the size of object (i.e., the nuclearity) is reduced. Thus, the core+*exo* cluster family exhibits a trend opposite to that of the conventional nanoparticles, which can be interpreted in terms of the jellium model. The increase in positive charge in the cluster jellium with the number of effective valence electrons kept constant (n^* = 4) can result in the more efficient stabilization of the HOMO electrons, leading to a wider gap between the HOMO/LUMO energies. Based on this model, the Au−Au distances of **1**−**3** would be affected by the nuclearity since electrons of the same number (4) are shared by the gold atoms in the cluster skeletons. The crystal structures showed that the core-to-*exo* distances were increased in the order **1** < **2** < **3**, whereas those in the cores were comparable to each other (Table S2).

Table 1. Lowest-Energy Optical Absorption and Photoluminescence Data of core+*exo*-type Clusters (1−3)[a]

		wavelength (nm)/energy (eV)	
cluster	nuclearity	absorption	photoluminescence[c]
1·$(NO_3)_2$	6	587/2.11[b]	–[d]
2·$(BF_4)_3$	7	556/2.23	642/1.93 (0.1%)
3·$(PF_6)_2$	8	508/2.44[b]	597/2.07 (0.1%)

[a]In MeOH at 25 °C. [b]Reproduced with permission from ref 20. Copyright (2013) American Chemical Society. [c]Excited at the absorption band. In parentheses, quantum efficiency relative to anthracene is given. [d]Only negligible photoluminescence was observed in the standard measurement region (600−750 nm).

Finally, we investigate the photoluminescence properties of **2**. We have previously reported that "core+*two*" Au_8 clusters (**3**) exhibit a photoluminescence band at ∼600 nm on excitation of the visible absorption band (∼510 nm).[12] Likewise, "core+*one*" Au_7 cluster (**2**·$(BF_4)_3$) with the same bitetrahedral Au_6 core showed a photoluminescence band at 642 nm ($\varphi \approx 0.1\%$) when excited at 555 nm (Figure 5b); the excitation spectrum (c) almost coincides with the absorption spectrum (a). The comparable Stokes shifts of **2** and **3** (∼0.3 eV) imply that their excited-state dynamics behaviors are virtually similar to each other and not dependent on the number of the *exo* gold atoms.

In conclusion, we have demonstrated the first example of a trivalent Au_7 cluster, thereby providing a missing link between Au_6 and Au_8 in the four-electron cluster family. Crystallographic structure determination showed that the "core+*exo*"-type geometry (*exo*-attached polyhedron) is a common structural feature of dppp-coordinated four-electron clusters. The structure of the Au_7 cluster is distinct from those of the Au_6 and Au_8 clusters in that it bears only *one exo* gold atom; however, the prolate shape was consistent with the theroretical prediction, thus supporting the validity of the structural jellium model. The tetrahedron-based core geometries of the four-electorn cluster family may have some relevance to the structure of a thiolate-capped Au_{24} cluster reported recently.[21] Absorption spectral profiles of Au_6, Au_7, and Au_8 clusters with "core+*exo*" structures provided a clear correlation between the cluster nuclearity and the first excitation energy. TD-DFT calculations revealed that the attachment of *only one* gold atom to a polyhedral core is sufficient to general unique electronic structure and optical features. This principle should be applicable to larger systems such as colloidal particles, which will benefit the rational design of functional nanometal modules.

■ ASSOCIATED CONTENT

Supporting Information

Details of synthesis, crystal data (cif file), computational results, and summary of the Au−Au bond distances of **2**·$(BF_4)_3$, and geometric structures of **1**−**3**. This material is available free of charge via the Internet at http://pubs.acs.org.

■ AUTHOR INFORMATION

Corresponding Author

konishi@ees.hokudai.ac.jp

Notes

The authors declare no competing financial interest.

■ ACKNOWLEDGMENTS

This work was partially supported by the MEXT/JSPS Grant-in-Aids (24350063 for K.K. and 24750001 for Y.S.), the Asahi Glass Foundation (K.K.), and the Sasakawa Scientific Research Grant and Tanaka Precious Metals Group (Y.S.). The authors also thank Mr. Qing Li for his contribution in the early stage of the work.

■ REFERENCES

(1) Jin, R. *Nanoscale* **2010**, *2*, 343−362. Tsukuda, T. *Bull. Chem. Soc. Jpn.* **2012**, *85*, 151−168.
(2) Mingos, D. M. P. *J. Chem. Soc., Dalton Trans.* **1976**, 1163−1169.
(3) Mingos, D. M. P.; Slee, T.; Lin, Z. Y. *Chem. Rev.* **1990**, *90*, 383−402.
(4) Walter, M.; Akola, J.; Lopez-Acevedo, O.; Jadzinsky, P. D.; Calero, G.; Ackerson, C. J.; Whetten, R. L.; Grönbeck, H.; Häkkinen, H. *Proc. Natl. Acad. Sci. U.S.A.* **2008**, *105*, 9157−9162.
(5) Shichibu, Y.; Negishi, Y.; Watanabe, T.; Chaki, N. K.; Kawaguchi, H.; Tsukuda, T. *J. Phys. Chem. C* **2007**, *111*, 7845−7847. Gutrath, B.; Oppel, I.; Presly, O.; Beljakov, I.; Meded, V.; Wenzel, W.; Simon, U. *Angew. Chem., Int. Ed.* **2013**, *52*, 3529−3532.
(6) Akola, J.; Walter, M.; Whetten, R. L.; Häkkinen, H.; Grönbeck, H. *J. Am. Chem. Soc.* **2008**, *130*, 3756−3757. Lopez-Acevedo, O.; Akola, J.; Whetten, R. L.; Grönbeck, H.; Häkkinen, H. *J. Phys. Chem. C* **2009**, *113*, 5035−5038. Zeng, C.; Qian, H.; Li, T.; Li, G.; Rosi, N. L.; Yoon, B.; Barnett, R. N.; Whetten, R. L.; Landman, U.; Jin, R. *Angew. Chem., Int. Ed.* **2012**, *51*, 13114−13118. Das, A.; Li, T.; Nobusada, K.; Zeng, Q.; Rosi, N. L.; Jin, R. *J. Am. Chem. Soc.* **2012**, *134*, 20286−20289.
(7) Hall, K. P.; Mingos, D. M. P. *Prog. Inorg. Chem.* **1984**, *32*, 237−325. Konishi, K. *Struct. Bonding (Berlin)* **2014**, DOI: 10.1007/430_2014_143.
(8) Hall, K. P.; Theoblad, B. R. C.; Gilmour, D. I.; Mingos, D. M. P.; Welch, A. J. *J. Chem. Soc., Chem. Commun.* **1982**, 528−530.
(9) Shichibu, Y.; Konishi, K. *Small* **2010**, *6*, 1216−1220. Shichibu, Y.; Suzuki, K.; Konishi, K. *Nanoscale* **2012**, *4*, 4125−4129. Briant, C. E.; Theobald, B. R. C.; White, J. W.; Bell, L. K.; Mingos, D. M. P.; Welch, A. J. *J. Chem. Soc., Chem. Commun.* **1981**, 201.
(10) Briant, C. E.; Hall, K. P.; Mingos, D. M. P.; Wheeler, A. C. *J. Chem. Soc., Dalton Trans.* **1986**, 687−692.
(11) Van der Velden, J. W. A.; Bour, J. J.; Steggerda, J. J.; Beurskens, P. T.; Roseboom, M.; Noordik, J. H. *Inorg. Chem.* **1982**, *21*, 4321−4324.
(12) Kamei, Y.; Shichibu, Y.; Konishi, K. *Angew. Chem., Int. Ed.* **2011**, *50*, 7442−7445. Kobayashi, N.; Kamei, Y.; Shichibu, Y.; Konishi, K. *J. Am. Chem. Soc.* **2013**, *135*, 16078−16081.
(13) Vollenbroek, F. A.; Bosman, W. P.; Bour, J. J.; Noordik, J. H.; Beurskens, P. T. *J. Chem. Soc., Chem. Commun.* **1979**, 387−388. Van der Velden, J. W. A.; Bour, J. J.; Bosman, W. P.; Noordik, J. H. *Inorg. Chem.* **1983**, *22*, 1913−1918. Yang, Y.; Sharp, P. R. *J. Am. Chem. Soc.* **1994**, *116*, 6983−6984.
(14) Schulz-Dobrick, M.; Jansen, M. *Angew. Chem., Int. Ed.* **2008**, *47*, 2256−2259.
(15) Briant, C. E.; Hall, K. P.; Mingos, D. M. P. *J. Chem. Soc., Chem. Commun.* **1984**, 290−292. Wen, F.; Englert, U.; Gutrath, B.; Simon, U. *Eur. J. Inorg. Chem.* **2008**, *2008*, 106−111.
(16) Briant, C. E.; Hall, K. P.; Wheeler, A. C.; Mingos, D. M. P. *J. Chem. Soc., Chem. Commun.* **1984**, 248−250. Pethe, J.; Maichle-Mössmer, C.; Strähle, J. *Z. Anorg. Allg. Chem.* **1998**, *624*, 1207−1210.
(17) Nunokawa, K.; Onaka, S.; Yamaguchi, T.; Ito, T.; Watase, S.; Nakamoto, M. *Bull. Chem. Soc. Jpn.* **2003**, *76*, 1601−1602. Gutrath, B. S.; Englert, U.; Wang, Y.; Simon, U. *Eur. J. Inorg. Chem.* **2013**, *2013*, 2002−2006.
(18) Shichibu, Y.; Kamei, Y.; Konishi, K. *Chem. Commun.* **2012**, *48*, 7559−7561.
(19) Van der Velden, J. W. A.; Beurskens, P. T.; Bour, J. J.; Bosman, W. P.; Noordik, J. H.; Kolenbrander, M.; Buskes, J. A. K. M. *Inorg. Chem.* **1984**, *23*, 146−151.
(20) Shichibu, Y.; Konishi, K. *Inorg. Chem.* **2013**, *52*, 6570−6575.
(21) Das, A.; Li, T.; Li, G.; Nobusada, K.; Zeng, C.; Rosi, N. L.; Jin, R. *Nanoscale* **2014**, *6*, 6458−6462.
(22) DFT and TD-DFT studies were performed with TURBOMOLE package (V6.3, 2011) in a similar manner to that described previously (ref 20 and Supporting Information).